

This article may be downloaded for personal use only. Any other use requires prior permission of the author and AIP Publishing.

The following article appeared in *Applied Physics Letters* 104, 191904 (2014); and may be found at <https://doi.org/10.1063/1.4876760>

High-quality InN films on MgO (100) substrates: The key role of 30° in-plane rotation

V. D. Compeán García, I. E. Orozco Hinostraza, A. Escobosa Echavarría, E. López Luna, A. G. Rodríguez, and M. A. Vidal

Citation: *Appl. Phys. Lett.* **104**, 191904 (2014);

View online: <https://doi.org/10.1063/1.4876760>

View Table of Contents: <http://aip.scitation.org/toc/apl/104/19>

Published by the [American Institute of Physics](#)

Articles you may be interested in

[Growth of HfO₂/TiO₂ nanolaminates by atomic layer deposition and HfO₂-TiO₂ by atomic partial layer deposition](#)

Journal of Applied Physics **121**, 064302 (2017); 10.1063/1.4975676

[Cubic GaN films grown below the congruent sublimation temperature of \(0 0 1\) GaAs substrates by plasma-assisted molecular beam epitaxy](#)

Journal of Vacuum Science & Technology B, Nanotechnology and Microelectronics: Materials, Processing, Measurement, and Phenomena **34**, 02L115 (2016); 10.1116/1.4943661

[Critical thickness of \$\beta\$ -InN/GaN/MgO structures](#)

Journal of Applied Physics **107**, 083510 (2010); 10.1063/1.3309757

[Indium nitride \(InN\): A review on growth, characterization, and properties](#)

Journal of Applied Physics **94**, 2779 (2003); 10.1063/1.1595135

[Structural characterization of AlGaAs:Si/GaAs \(631\) heterostructures as a function of As pressure](#)

Journal of Vacuum Science & Technology B, Nanotechnology and Microelectronics: Materials, Processing, Measurement, and Phenomena **34**, 02L119 (2016); 10.1116/1.4944452



Scilight

Sharp, quick summaries **illuminating**
the latest physics research

Sign up for **FREE!**

AIP
Publishing

High-quality InN films on MgO (100) substrates: The key role of 30° in-plane rotation

V. D. Compeán García,¹ I. E. Orozco Hinostriza,² A. Escobosa Echavarría,³
 E. López Luna,¹ A. G. Rodríguez,¹ and M. A. Vidal¹

¹Coordinación para la Innovación y Aplicación de la Ciencia y Tecnología (CIACyT),
 Universidad Autónoma de San Luis Potosí (UASLP), Álvaro Obregón 64, 78000 San Luis Potosí, Mexico

²Instituto Potosino de Investigación Científica y Tecnológica, Camino a la Presa San José 2055,
 Col. Lomas 4a Sección, 78216 San Luis Potosí, Mexico

³Electric Engineering Department, Centro de Investigación y Estudios Avanzados del IPN,
 Apartado Postal 14-740, 07000 México D.F., Mexico

(Received 21 February 2014; accepted 3 May 2014; published online 14 May 2014)

High crystalline layers of InN were grown on MgO(100) substrates by gas source molecular beam epitaxy. Good quality films were obtained by means of an in-plane rotation process induced by the annealing of an InN buffer layer to minimize the misfit between InN and MgO. *In situ* reflection high-energy electron diffraction showed linear streaky patterns along the [01 $\bar{1}$ 0] azimuth and a superimposed diffraction along the [11 $\bar{2}$ 0] azimuth, which correspond to a 30° α -InN film rotation. This rotation reduces the mismatch at the MgO/InN interface from 19.5% to less than 3.5%, increasing the structural quality, which was analyzed by high-resolution X-ray diffraction and Raman spectroscopy. Only the (0002) *c* plane diffraction of α -InN was observed and was centered at $2\theta = 31.4^\circ$. Raman spectroscopy showed two modes corresponding to the hexagonal phase: E1(LO) at 591 cm^{-1} and E2(high) at 488 cm^{-1} . Hall effect measurements showed a carrier density of $9 \times 10^{18}\text{ cm}^{-3}$ and an electron Hall mobility of $340\text{ cm}^2/(\text{V s})$ for a film thickness of 140 nm. © 2014 AIP Publishing LLC. [<http://dx.doi.org/10.1063/1.4876760>]

Over the last few years, the hexagonal and cubic phases of the semiconductor InN have attracted much interest from both fundamental and practical points of view. The interest in this semiconductor and the complete III-nitride alloy system increased after the correct determination of the fundamental band-gap energy of InN from the original value of 1.9 (Ref. 1) to 0.67 eV,²⁻⁴ which meant that InN has the lowest band gap of any known III-nitride binary compound or alloy. This extended the expected emission range of III-nitride alloys from deep-UV (AlN) down to the near-IR region (InN). InN also exhibits exceptional transport properties, such as a very small electron effective mass at the Γ point ($0.07 m_0$), which may lead to high electron mobilities, high saturation velocities, a pronounced band-filling effect in samples with electron concentrations in the order of 10^{18} – 10^{19} cm^{-3} ,³ a surface accumulation layer with ultra-high electron density, and very high saturation and peak drift velocities.⁵⁻⁷ These unique properties make InN a potential material for a wide range of devices, such as tandem solar cells, infrared emitters, and high-speed and high-frequency electronic devices. As a consequence, a great deal of effort has been dedicated to improving the crystal quality of InN layers using different substrates to grow high-quality InN and its InGaIn alloys, and numerous studies of the optical and electrical properties of InN can be found in the literature.¹⁻⁸

One of the problems of III-nitride systems is that no native substrates exist; for example, InN has a lattice mismatch of 25% with sapphire, 8% with Si(111), 37.4% with GaAs, and 11% with GaN. High-quality single-crystal InN is very difficult to obtain because of this. Magnesium oxide (MgO) has been used to grow cubic InN with a buffer layer

of cubic gallium nitride (β -GaN),⁹⁻¹¹ because of the large lattice mismatch between InN(100) and MgO(100) of $\sim 18\%$. If a buffer layer of GaN is not used then poor-quality polycrystalline α -InN is obtained.^{9,12}

In this study, we report the growth of high-quality α -InN and discuss the effect of annealing on the low-temperature (LT)-InN buffer layer. In addition, we characterize the structural quality of the α -InN by *in situ* and real-time reflection high-energy electron diffraction (RHEED), X-ray diffraction (XRD), and Raman spectroscopy.

InN films were grown by gas source molecular beam epitaxy (GS-MBE) on (100)-oriented MgO substrates using an InN buffer layer grown at a low substrate temperature (LT) of $T_s = 300^\circ\text{C}$, as described in the next section.

The *in situ* real-time surface characterization was performed by RHEED with an acceleration voltage of 12 kV. Atomic Force Microscopy (AFM) in tapping mode was used to study surface morphology. The structural properties were studied using a high-resolution X-ray diffraction (HRXRD) system with a PANalytical MRD X-ray diffractometer, using the $K\alpha_1$ line emission (1.54059 \AA) from a Cu target as the X-ray source and a 2 bounce hybrid monochromator made of a (220) germanium crystal. The voltage and applied current were fixed at 40 mV and 20 mA, respectively. Room temperature Raman spectra were measured with a 514.5 nm excitation laser line and the electrical properties were evaluated by Hall measurements in the van der Pauw configuration system at 300 K.

Before growing LT-InN, the substrate was cleaned in a trichloroethylene and acetone ultrasonic bath for 10 min. The MgO substrate was introduced into a vacuum chamber and was then transferred to the growth chamber and thermally

cleaned in a high vacuum environment ($\sim 3 \times 10^{-8}$ Torr) at $T_s = 600^\circ\text{C}$ for 30 min to obtain a clean and atomically flat surface, as can be seen from the RHEED pattern shown in Fig. 1(a). The substrate temperature was then lowered to $T_s = 300^\circ\text{C}$ to deposit the LT-InN buffer layer. The surface of the MgO substrate was exposed to indium flux with a cell temperature of 830°C and nitrogen plasma with N_2 flow at a rate of 1.6 standard cubic centimeters per minute and a radio frequency power of 215 W for a period of 5 min. Fig. 1(b) shows the $[01\bar{1}0]$ azimuth RHEED pattern of α -InN with a spotty configuration characteristic of a three-dimensional (3D) layer, which is a diagram of the crystallographic directions of the InN. Then, the indium cell was closed and the temperature T_s was increased to 500°C for 20 min to anneal the LT-InN layer and recrystallize and remove any unreacted In on the InN surface [Fig. 1(c)] (20 min was chosen when the rotation process was observed in the RHEED pattern). At the end of the annealing process, a layer of InN was grown for 120 min under the same conditions. A good surface was obtained, as shown by atomic force microscopy with different crystals rotated by 30° [Fig. 1(d)].

To gain insight into the inter-planar adjustment between InN and MgO, it is necessary to discuss the following sequence of events: (i) at the start, a streaky RHEED pattern indicating a two-dimensional surface morphology was observed for the MgO surface; (ii) the original cubic $[100]$ azimuth of MgO disappeared when the first monolayers of InN were deposited, the RHEED pattern disappeared, and only the hexagonal $[01\bar{1}0]$ azimuth remained; (iii) after annealing, the $[11\bar{2}0]$ azimuth overlapped with the $[01\bar{1}0]$ azimuth, as indicated by the spotty RHEED pattern, which corresponds to a 30° rotation of the α -InN film; and (iv) at the end of growth, a streaky RHEED pattern was observed [Fig. 2(a)]. Fig. 2(b) shows an intensity profile of the diffraction pattern. The distance between $x = -1$ and $x = 1$ represents the distance between the diffraction bars of $(0, -1)$ and $(0, 1)$, corresponding to the lattice constant of α -InN in real

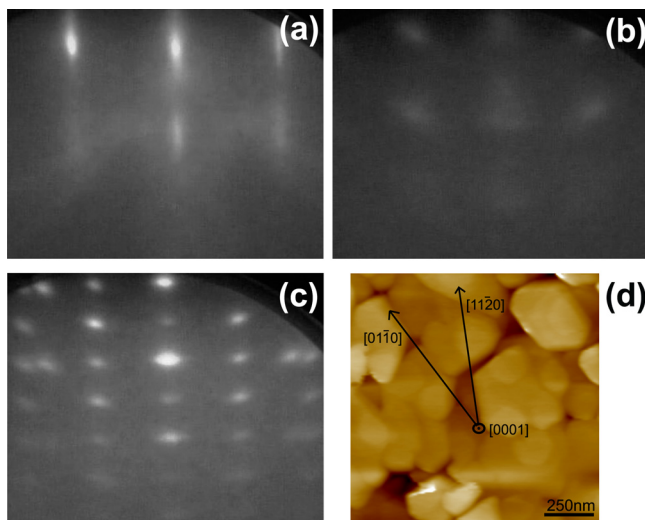


FIG. 1. RHEED patterns (a) along the $[100]$ azimuth of the MgO substrate at the end of the cleaning process, (b) along $[01\bar{1}0]$ of InN after the deposition of the LT-InN buffer layer, (c) along the $[01\bar{1}0]$ azimuth after the annealing treatment at $T_s = 500^\circ\text{C}$ for 20 min, and (d) AFM image at the end of 2 h growth.

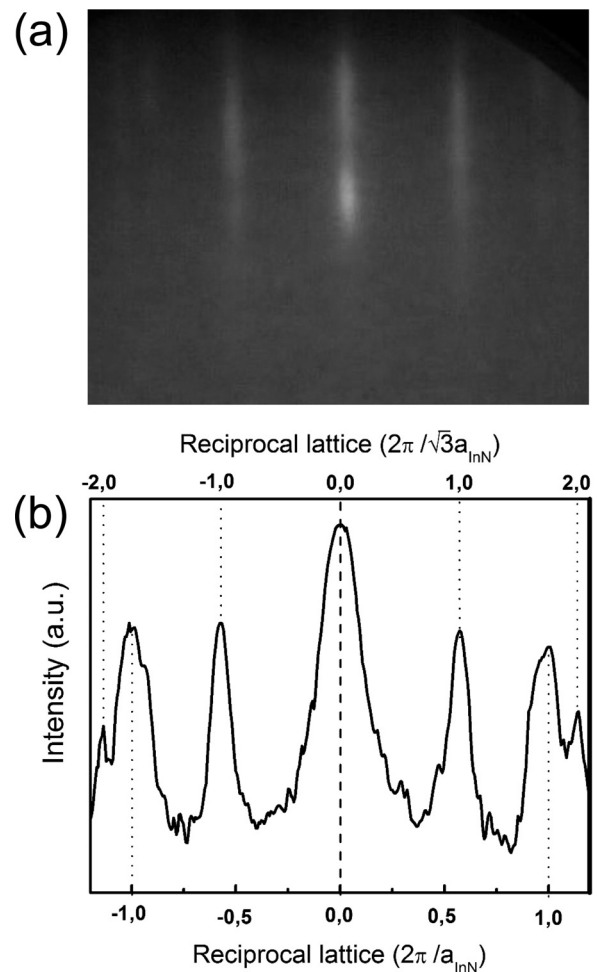


FIG. 2. (a) RHEED pattern taken along the $[01\bar{1}0]$ azimuth from the InN surface at the end of 2 h growth and (b) intensity profiles of the RHEED patterns of (a).

space ($a_{\text{InN}} = 0.356$ nm), which is equivalent to the $[01\bar{1}0]$ azimuth of InN. In the upper x -axis, the distance from $x = -1$ to $x = 1$ corresponds to a distance of $\sqrt{3}a_{\text{InN}} = 0.608$ nm along the $[11\bar{2}0]$ azimuth in real space, which is a rotation of 30° with respect to the $[01\bar{1}0]$ direction, as shown in Figs. 2(a) and 2(b). A model of the rotation of InN over MgO in real space is shown in Fig. 3(a). It is possible to observe the formation of two domains oriented in the $[01\bar{1}0]$ and $[11\bar{2}0]$ azimuths, where the In atoms adjust on O atoms in the $[11\bar{2}0]$ oriented domain and In atoms adjust on both Mg and O atoms of the MgO (001) surface for the $[01\bar{1}0]$ domain of the InN film.

After the annealing process of LT-InN, any unreacted In on the InN surface was removed and then the structure recrystallized via an in-plane rotation of 30° to minimize strain and reach the minimum energy. Thermodynamically, this process is favorable owing to a decrease in the system mismatch from 19.5% for $[01\bar{1}0]$ InN/ $[110]$ MgO to 3.5% for $[11\bar{2}0]$ InN/ $[110]$ MgO. The coexisting of two crystalline domains was formed: one of them maintained a high lattice mismatch (19.5%) and the other one a low lattice mismatch (3.5%) between MgO substrate and InN film. The growth of InN has a hexagonal mosaic form, as can be observed in Fig. 1(d), and it is also possible to observe hexagonal mosaics rotated by 30° among them.

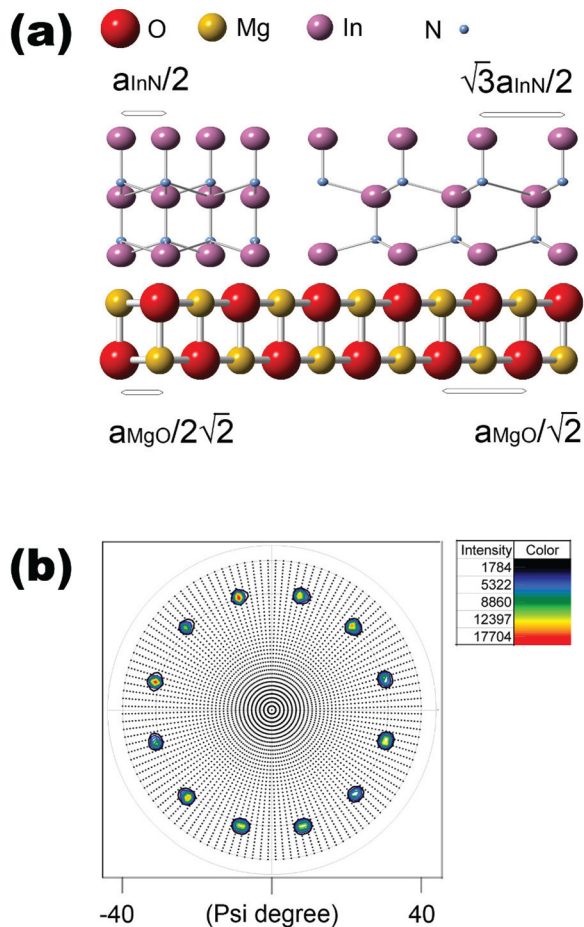


FIG. 3. (a) Real-space model of the MgO/LT-InN interface and (b) a pole diagram taken in the $(10\bar{1}1)$ plane of InN showing 12-fold symmetry.

To examine the formation of domains oriented in the $[11\bar{2}0]$ and $[01\bar{1}0]$ directions, and confirm the presence of this rotated plane, a pole diagram was obtained by HRXRD at $2\theta = 33.1^\circ$, corresponding to the $(10\bar{1}1)$ plane of α -InN, as shown in Fig. 3(b). The film-tilt angle ψ was varied in the range of 0° – 80° in steps of 2° , and the azimuth angle was varied from 0° to 360° in steps of 3° . A 12-fold symmetry structure was observed, showing the two hexagonal domains with 30° plane rotation.

Fig. 4(a) shows a rocking curve of α -InN for the in-growth planes. The α -InN diffraction peak of the (0002) c -plane is clearly observed at $2\theta = 31.4^\circ$ with a full-width at half maximum (FWHM) of 0.24° and the diffraction peak corresponding to the (002) plane of the MgO substrate is observed at $2\theta = 43^\circ$.

A typical Raman spectrum is shown in Fig. 4(b). Two phonon structures at frequencies of 488 and 591 cm^{-1} are observed and are identified as the E2(high) and the E1(LO) phonons, respectively. These peaks correspond to the InN wurtzite bulk phonon frequencies.¹³ The FWHM of the E2(high) Raman peak is broadened by the lattice disorder that disturbs the phonon correlation length, mainly by the formation of nanocrystals or the presence of defects and impurities.¹⁴ The typical FWHM of the E2(high) phonon in this work was 9 cm^{-1} , which is comparable to the values of 7 and 8 cm^{-1} for InN grown on Si(111) (Ref. 15) and Al_2O_3 ,¹⁶ respectively, indicating the good crystalline quality of the α -InN film.

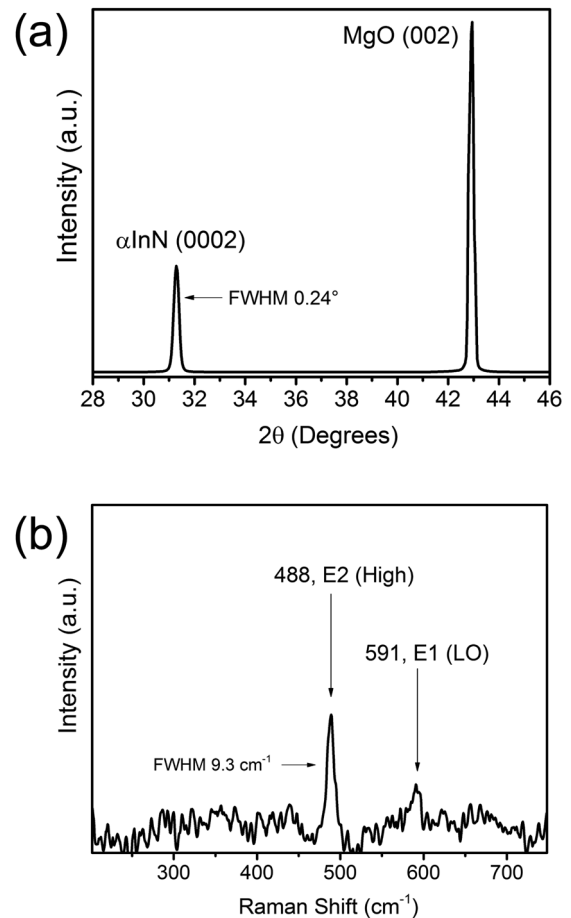


FIG. 4. (a) X-ray rocking curves of InN/MgO(001) and (b) Raman spectrum of InN film.

Room temperature Hall effect measurements reveal an unintentional n-type doped InN film with a carrier density of $9 \times 10^{18}\text{ cm}^{-3}$ and an electron Hall mobility of $340\text{ cm}^2/(\text{V s})$. This mobility is the highest value reported for InN films with a thickness of about 140 nm,⁵ indicating the very good crystalline quality of the material reported in this work.

The growth of InN without the annealing process of the LT-InN buffer layer generates a mixture of phases. The first phase is wurtzite, the well-known stable structure of InN, and the system tends to the minimum energy and the hexagonal phase is naturally generated. However, the system also attempts to follow the cubic structure of the MgO substrate, creating cubic phase InN domains between the wurtzite domains. Owing to this mixture of phases, the layer undergoes 3D growth with a high number of defects affecting the structural quality of the film, in contrast to the very good quality films obtained with the annealed LT-InN buffer layer.

In summary, we grown high crystalline quality hexagonal InN films directly on MgO(100) substrates with a LT-InN buffer layer by GS-MBE. RHEED analysis showed that InN grows with two crystal orientations as $[01\bar{1}0]$ InN/ $[110]$ MgO and $[11\bar{2}0]$ InN/ $[110]$ MgO, decreasing the lattice mismatch from 19.5% to 3.5%. The LT-InN buffer layer was annealed for 20 min at 500°C to achieve recrystallization and induce plane rotation. In addition, a pole diagram was obtained in the $(10\bar{1}1)$ InN plane, showing 12-fold symmetry with the two hexagonal domains with 30° in-plane rotation.

Structural characterization by XRD revealed the diffraction peak of α -InN at the (0002) plane, and Raman spectroscopy showed the E2(high) phonon with a FWHM of 9 cm^{-1} .

Thus, we have obtained high-quality InN films using the surface properties of MgO(100) to reduce the mismatch between the InN film and MgO substrate.

¹T. L. Tansley and C. P. Foley, *J. Appl. Phys.* **59**, 3241 (1986).

²J. Wu, W. Walukiewicz, K. M. Yu, J. W. Ager, E. E. Haller, H. Lu, W. J. Schaff, Y. Saito, and Y. Nanishi, *Appl. Phys. Lett.* **80**, 3967 (2002).

³W. Walukiewicz, J. W. Ager III, K. M. Yu, Z. Liliental-Weber, J. Wu, S. X. Li, R. E. Jones, and J. D. Denlinger, *J. Phys. D* **39**, R83 (2006)

⁴M. Higashiwaki and T. Matsui, *J. Cryst. Growth* **162**, 269 (2004).

⁵A. Knübel, R. Aidam, V. Cimalla, L. Kirste, M. Bäumler, C.-C. Leancu, V. Lebedev, J. Wallauer, M. Walther, and J. Wagner, *Phys. Status Solidi C* **6**(6), 1480–1483 (2009).

⁶S. K. O'Leary, B. E. Foutz, M. S. Shur, and L. F. Eastman, *Appl. Phys. Lett.* **88**, 152113 (2006).

⁷S. K. O'Leary, B. E. Foutz, M. S. Shur, and L. F. Eastman, *Appl. Phys. Lett.* **87**, 222103 (2005).

⁸W.-C. Chen and S.-Y. Kuo, *J. Nanomater.* **2012**, 853021.

⁹Y. Iwahashi, H. Yaguchi, A. Nishimoto, M. Orihara, Y. Hijikata, and S. Yoshida, *Phys. Status Solidi C* **3**(6), 1515–1518 (2006).

¹⁰M. Perez Caro, A. G. Rodríguez, E. López-Luna, M. A. Vidal, and H. Navarro-Contreras, *J. Appl. Phys.* **107**(8), 083510 (2010).

¹¹S. Sanorpim, S. Kuntharin, J. Parinyataramas, H. Yaguchi, Y. Iwahashi, M. Orihara, Y. Hijikata, and S. Yoshida, *AIP Conf. Proc.* **1399**, 131 (2011).

¹²H. Navarro-Contreras, M. Pérez Caro, A. G. Rodríguez, E. López-Luna, and M. A. Vidal, *Rev. Mex. Fís.* **58**, 144–151 (2012).

¹³T. Inushima, T. Shiraishi, and V. Yu Davydov, *Solid State Commun.* **110**, 491–495 (1999).

¹⁴K. K. Tiong, P. M. Amirtharaj, F. H. Pollak, and D. E. Aspnes, *Appl. Phys. Lett.* **44**, 122 (1984).

¹⁵F. Agullo-Rueda, E. E. Mendez, B. Bojarczuk, and S. Guha, *Solid State Commun.* **115**, 19–21 (2000).

¹⁶J. B. Wang, Z. F. Li, P. P. Chen, Wei Lu, and T. Yao, *Acta Mater.* **55**, 183–187 (2007).